*Supporting Information*

# Heterogeneous formation and light absorption of secondary organic aerosols from acetone photooxidation: Remarkably enhancing effects of seeds and ammonia

Si Zhang[1], Xinbei Xu[1], Luyao Chen[1], Can Wu[1,2], Zheng Li[1], Rongjie Li[1], Binyu Xiao[1], Xiaodi Liu[1], Rui Li[1,2], Fan Zhang[1,2], Gehui Wang[1,2]*

[1]Key Lab of Geographic Information Science of the Ministry of Education, School of Geographic Sciences, East China Normal University, Shanghai 200241, China

[2] Institute of Eco-Chongming, 20 Cuiniao Rd., Chongming, Shanghai 202150, China

*Corresponding author: Prof. Gehui Wang, Email: ghwang@geo.ecnu.edu.cn

Tel: 86-21-54341193, Fax: 86-21-54341122

This PDF file includes:

1. Supplementary Text S1-S6
2. Seven figures, Figure S1-S8
3. Three tables, Table S1-S3
4. References

**Text S1. Particle wall loss correction**

The particle wall loss was corrected by using a total-mass-concentration-based method (Liu and Abbatt, 2021). The wall-loss-corrected sulfate concentration at time t $wC_{so_4^{2-}}(t)$ can be calculated using the Eq.(1).

$$wC_{so_4^{2-}}(t) = C^{sus}_{so_4^{2-}}(t) + k\int_0^t C^{sus}_{so_4^{2-}}(t)dt \qquad (1)$$

where $C^{sus}_{so_4^{2-}}(t)$ is the measured sulfate concentration at time t, and k is the first order particles wall loss rate constant, $1\times10^{-4}$ $s^{-1}$ in this study. The wall loss rate constants of pure $(NH_4)_2SO_4$ seed and $NH_4NO_3$ seed were similar under the experimental conditions in this work.

**Text S2. $NH_3$ concentration wall loss correction**

According to the reports of Huang et al. (2018)and Zhang et al. (2014), the vapor wall loss of gas compounds in Teflon-walled chambers can be estimated by a two-layer model, and the overall mass transport coefficient across the gas-phase boundary layer and the air-Teflon interface can be calculated by Eq.2-4. Then the first-order wall loss coefficient ($k_w$) can be calculated by Eq.5. Therefore, the loss of $NH_3$ to the chamber wall is estimated by the $k_w$ by considering the gas-phase transport within the chamber, as reported by Zhang et al. (2014)

$$v_1 = \left(\frac{1}{v_e} + \frac{1}{v_c}\right)^{-1} \qquad (2)$$

$$v_e = \frac{2}{\pi}\sqrt{k_e \mathcal{D}_g} \qquad (3)$$

$$v_c = \frac{\alpha_w \omega}{4} \qquad (4)$$

$$k_w = \left(\frac{A}{V}\right)v_1 = \left(\frac{A}{V}\right)\frac{\alpha_w\omega}{4+\frac{\pi}{2}\left(\frac{\alpha_w\omega}{\sqrt{k_e D_g}}\right)} \qquad (5)$$

where A/V is the surface-to-volume ratio of the chamber; $\alpha_w$ is the mass accommodation coefficient of $NH_3$ onto the Teflon chamber walls at RH = 90% (0.01) (Bongartz et al., 1995); ω is the mean molecular speed of $NH_3$ (603 m $s^{-1}$) (Seinfeld and Pandis, 2006); $k_e$ is the

coefficient of eddy diffusion and is estimated to be 0.31 for the chamber used in this work; $D_g$ is the gas-phase diffusion coefficient ($1.98\times 10^{-5}$) (Tang et al., 2014).

Therefore, the loss of $NH_3$ to the chamber wall is estimated by the $k_w$ by considering the gas-phase transport within the chamber (Zhang et al., 2014). The average concentration of $NH_3$ is estimated by eq. 6,

$$[\overline{NH_3}]=\frac{1-e^{-k_w\Delta t}}{k_w\Delta t}[NH_3]_0 \quad (6)$$

where the first-order wall-loss coefficient ($k_w$) of $NH_3$ in this study is $9.5 \times 10^{-3}$ $s^{-1}$ and $\Delta t$ is the reaction time. For an initial injection concentration of 1250 ppbv $NH_3$, the average concentration of $NH_3$ in the chamber was corrected to be 73 ppbv.

**Text S3. VOCs concentration wall loss correction and estimation of MGly concentration**

The vapor wall loss coefficients of VOCs in chamber were also calculated by Eq.2. The values of $\alpha_w$, $k_e$, $\omega$ and $D_g$ of VOCs were calculated by eq.7-10, respectively (Huang et al., 2018).

$$\alpha_w = 10^{-2.744}(c^*)^{-0.6566} \quad (7)$$

$$\log_{10}c^* = (n_C^0 - n_C)b_C - n_O b_O - 2\frac{n_C n_O}{n_C + n_O}b_{CO} - n_N b_N - n_S b_S, \quad (8)$$

$$k_e = 0.004 + 10^{-2.25}(V)^{0.74} \quad (9)$$

$$\omega = \sqrt{\frac{8RT}{\pi MW_{voc}}} \quad (10)$$

where $c^*$ is the vapor saturation concentration of VOCs, and the calculation method and all parameters were explained in detail by Li et al. (2016); R is the gas constant, 8.314 (kg $m^2$ $s^{-2}$ $K^{-1}$ $mol^{-1}$); T is the temperature; $MW_{voc}$ is the vapor molecular weight of VOCs; $D_g$ of VOCs were referred to the results of Tang et al. (2015).

In this study, the concentrations of MGly measured by PTR-MS were the equilibrium concentrations after gas-particle partitioning and multiphase reactions, which would underestimate the contribution of MGLY in the SOA formation. Hence, the total

concentrations of MGly in gas phase were estimated through the molar yield (14%) of MGLY in acetone-OH oxidation reported by Fu et al. (2008). Then the total concentrations of MGly were vapor wall loss corrected by $k_w$.

**Text S4. Concentration of OH radicals**

In this study, the concentration of OH was estimated from exponential fitting of the measured decay of acetone concentration (eq.11-12) (Li et al., 2021a)

$$[\text{Acetone}] = [\text{Acetone}]_0 e^{-k2t} \quad (11)$$

$$[OH] = \frac{k_2}{k_1} \quad (12)$$

where $[\text{Acetone}]_0$ is the initial concentration of acetone and $k_2$ is the fitted pseudo first-order rate constant for the acetone-OH reaction, and $k_1$ ($5.5 \times 10^{-12}$ $cm^3$ $molecule^{-1}$ $s^{-1}$) is the reaction rate between OH and acetone. The calculated concentrations of [OH] are about $5.3 \times 10^8$ molecules $cm^{-3}$.

**Text S5. The calculation of the MAC of SOA**

In this study, the light absorption coefficient ($Abs_\lambda$, M $m^{-1}$) and the mass absorption coefficient ($MAC_\lambda$, $m^2$ $g^{-1}$) at the wavelength of λ of SOA were calculated using eq.13 and 14, respectively (Liu et al., 2023).

$$\text{Abs}_\lambda = (A_\lambda - A_{700}) \frac{V_w}{V_a \times l} \times \ln(10) \quad (13)$$

$$\text{MAC}_\lambda = \frac{\text{Abs}_\lambda}{M} \quad (14)$$

where $A_\lambda$ and $A_{700}$ represent the light absorption at the wavelengths of λ and 700 nm measured by LWCC, respectively; $V_w$ and $V_a$ represent the volume of solvent and the volume of air corresponding to the filter punch, respectively; and l is the absorbing path length (1 m); M is the concentration of water-soluble organic carbon (WSOC, μgC $m^{-3}$).

**Text S6. The calculation of the partition coefficients of $NH_3$ ($\varepsilon(NH_4^+)$)**

The partition coefficients of $NH_3$ ($\varepsilon(NH_4^+)$) on different seeds were calculated by eq.15 and 16 (Guo et al., 2017; Nah et al., 2018).

$$\varepsilon(NH_4^+) \cong \frac{\frac{\gamma_{H^+}10^{-pH}}{\gamma_{NH_4^+}} H^*_{NH_3} W_i RT \times 0.987 \times 10^{-14}}{1 + \frac{\gamma_{H^+}10^{-pH}}{\gamma_{NH_4^+}} H^*_{NH_3} W_i RT \times 0.987 \times 10^{-14}} \quad (15)$$

$$\ln(H^*_{NH_3}) = 25.393 - 10373.6(1/T_r - 1/T) + 4.131(T_r/T - (1 + \ln(T_r/T))) \quad (16)$$

where $\gamma_{H^+}$ and $\gamma_{NH_4^+}$ are activity coefficients of $H^+$ and $NH_4^+$, respectively, calculated from E-AIM model; $H^*_{NH_3}$ is equilibrium constants calculated by eq.16; R is the gas constant; T is temperature; $W_i$ is particle liquid water content associated with inorganic species.

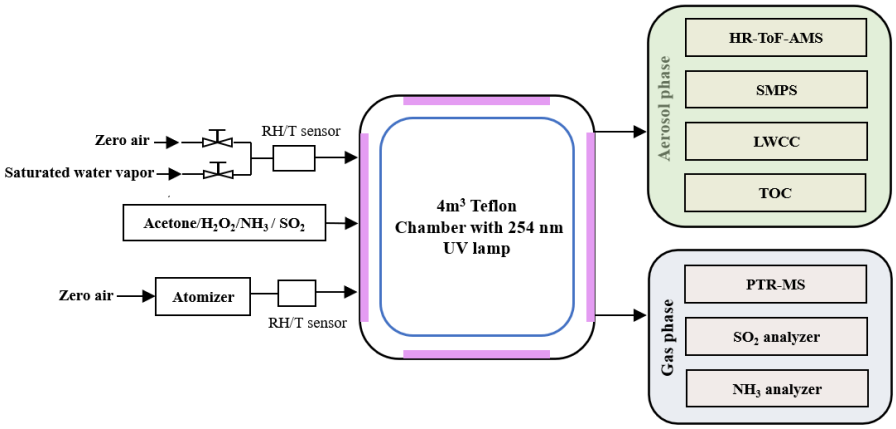


95

96 **Figure S1.** A schematic diagram of experimental setup in this work

97

98

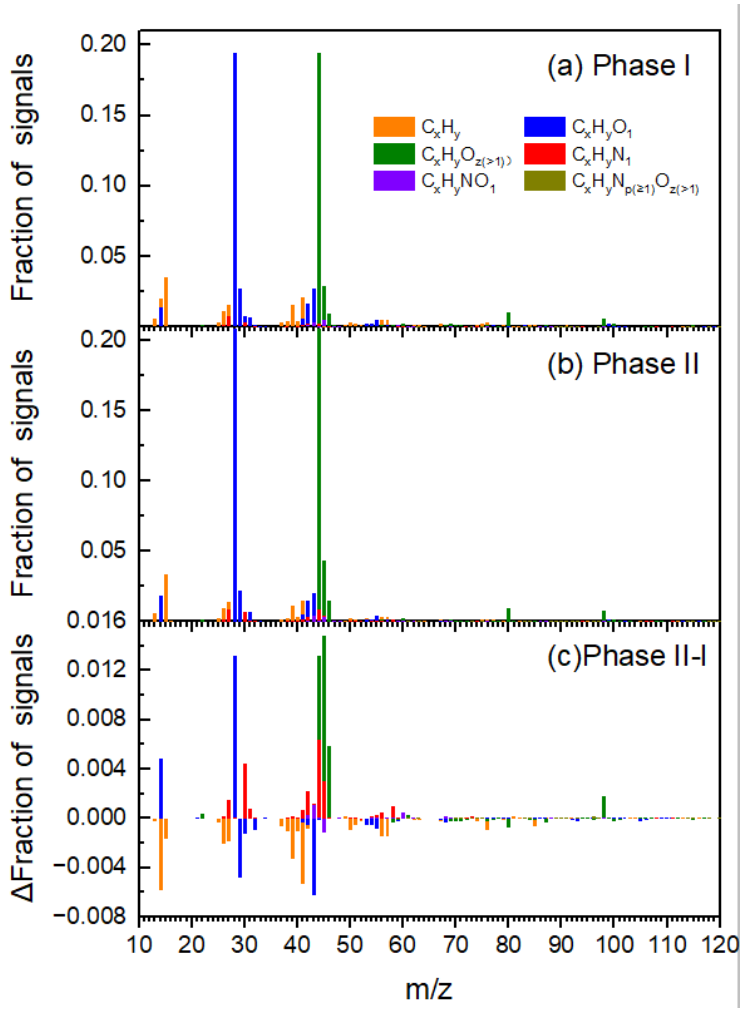


99

100 **Figure S2.** The mass spectra of acetone-derived SOA measured by HR-AMS during
101 the Phase I and Phase II (a and b) and their difference between the two phases (c). Data
102 were taken and analyzed at a high resolution but were summarized to a unit mass
103 resolution for display.

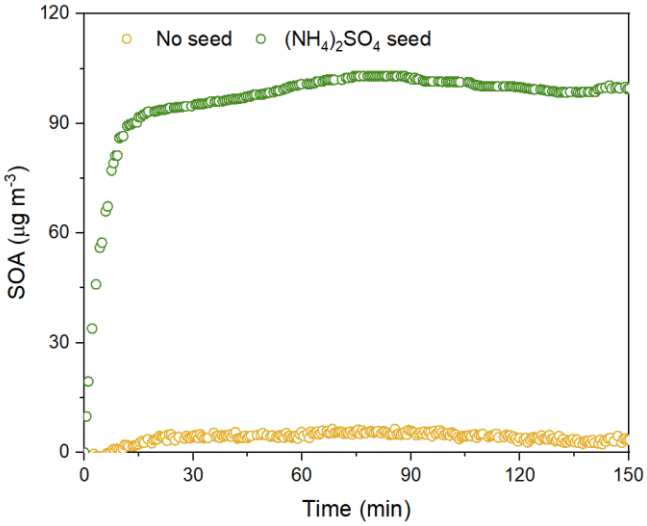


**Figure S3.** Concentrations of acetone-derived SOA in the chamber during the Phase I as a function of reaction time in the absence and presence of $(NH_4)_2SO_4$ seeds, respectively.

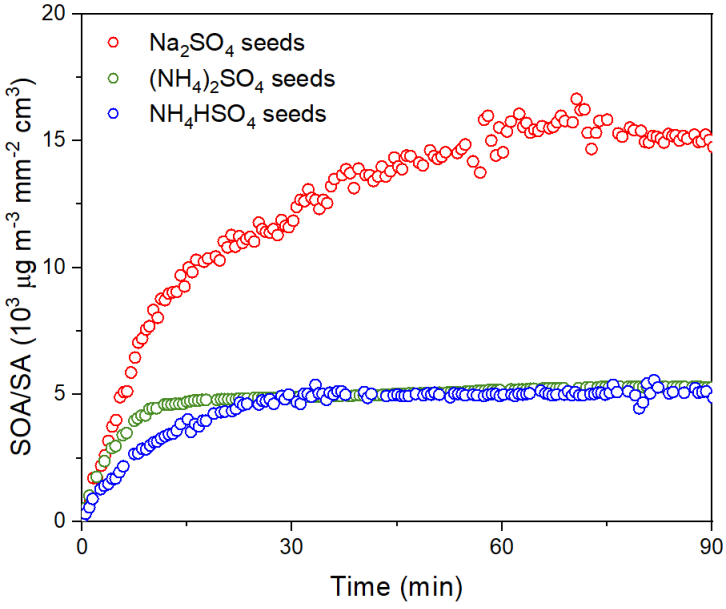


**Figure S4.** Normalized concentrations of SOA to the surface area (SA) of different seeds at Phase I as a function of reaction time during the exposure of various seeds to 750 ppb acetone and $5.3 \times 10^8$ molecules $cm^{-3}$ OH radicals under 85% RH.

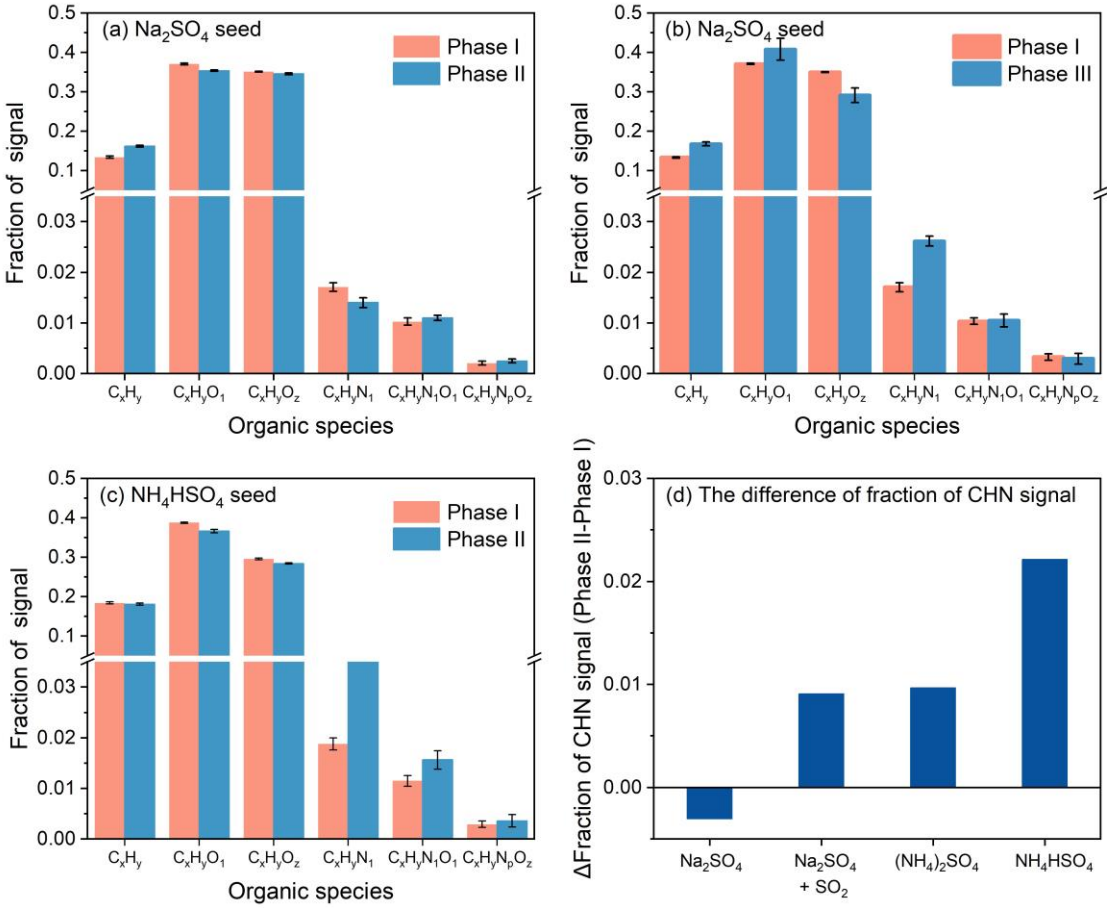


**Figure S5.** (a-c) The fraction of various organic species family signal of acetone-derived SOA at different reaction phases. (Phase I: Photooxidation of acetone by OH radicals without $NH_3$; Phase II: Reaction of acetone oxidation products with $NH_3$ under dark conditions; Phase III: Addition of 500 ppb $SO_2$ into the chamber after Phase II in the presence of $Na_2SO_4$ seeds); (d) The enhancement of the fraction of CHN ions family of Phase II over Phase I on different seeds (the value on $Na_2SO_4$ seed with $SO_2$ is the enhancement of Phase III over Phase I).

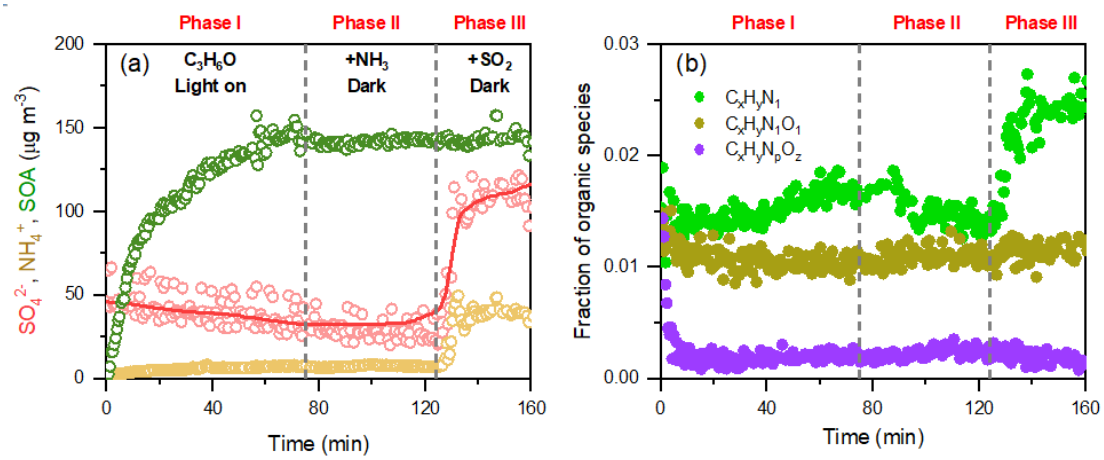


**Figure S6.** (a) The mass concentration of SOA, $NH_4^+$ and $SO_4^{2-}$ during the reaction given by HR-ToF-AMS, which were corrected according to the results of SMPS; (b) The variations of fractions of N-containing organic species signals during the reaction on $Na_2SO_4$ seed with $NH_3$ and $SO_2$.

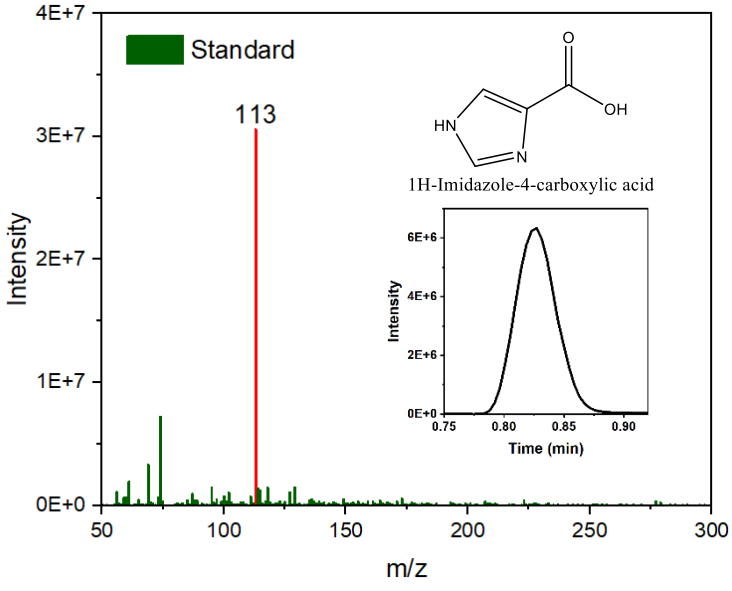


**Figure S7.** The ESI-Orbitrap MS spectra of the 1H-Imidazole-4-carboxylic acid standard.

**Table S1.** Initial conditions of the experiments

| Exp. No. | Acetone (ppb) | OH[a] (molecules $cm^{-3}$) | $NH_3$ (ppb) | $SO_2$ (ppb) | Seeds | RH (%) |
|---|---|---|---|---|---|---|
| 1 | 750 | $5.3 \times 10^8$ | 73 | / | $(NH_4)_2SO_4$ | 85±1 |
| 2 | 750 | $5.3 \times 10^8$ | 73 | / | $(NH_4)HSO_4$ | 85±1 |
| 3 | 750 | $5.3 \times 10^8$ | 73 | / | $Na_2SO_4$ | 85±1 |
| 4 | 750 | $5.3 \times 10^8$ | 73 | 500 | $Na_2SO_4$ | 85±1 |
| 5 | 750 | $5.4 \times 10^8$ | 73 | / | / | 85±1 |

[a] The concentrations of OH radicals in all experiments were calculated by Text S4.

**Table S2.** ESI-Orbitrap MS measured products in acetone SOA

| Measured Mass $[M+H]^+$ | Theory Mass | Suggested Formula | Molecular Structure | Seeds | Ref. |
|---|---|---|---|---|---|
| 72 | 71 | $C_3H_5NO$ | 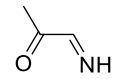 | $(NH_4)_2SO_4$ | De Haan et al. (2019) |
| 163 | 162 | $C_6H_{10}O_5$ | 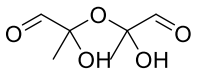 | | Li et al. (2021b) |
| 195 | 194 | $C_9H_{10}N_2O_3$ | 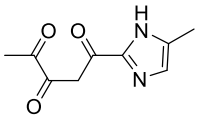 | | Aiona et al. (2017) |
| 235 | 234 | $C_9H_{14}O_7$ | 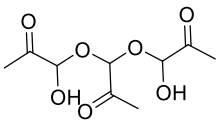 | | Li et al. (2021b) |
| 341 | 340 | $C_{15}H_{20}O_7N_2$ | 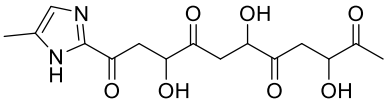 | | Aiona et al. (2017) |
| 105 | 104 | $C_3H_4O_4$ | 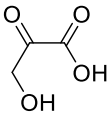 | $Na_2SO_4$ | Altieri et al. (2008) |
| 119 | 118 | $C_4H_6O_4$ | 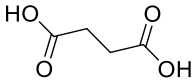 | | Altieri et al. (2008) |
| 135 | 134 | $C_4H_6O_5$ | 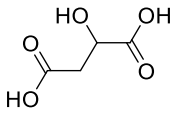 | | Altieri et al. (2008) |
| 161 | 160 | $C_6H_8O_5$ | 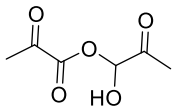 | | |
| 179 | 178 | $C_6H_{10}O_6$ | 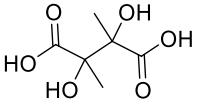 | | Guzmán et al. (2006) |
| 217 | 216 | $C_9H_{12}O_6$ | 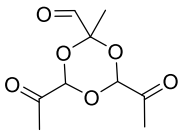 | | Zhao et al. (2006) |
| 233 | 232 | $C_9H_{12}O_7$ | 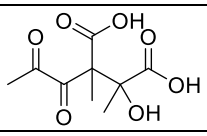 | | Tan et al. (2012) |

**Table S3** Concentrations of total SOA formed in the chamber and that formed only from the uptake of methylglyoxal (MGly) in the chamber

| Seed | SOA[a] ($\mu g\ m^{-3}$) | Surface area of seeds ($m^2\ m^{-3}$) | MGly ($\mu g\ m^{-3}$) | $\gamma$[b] | $SOA_{MGly}$[c] ($\mu g\ m^{-3}$) | $SOA/SOA_{MGly}$ |
|---|---|---|---|---|---|---|
| $Na_2SO_4$ | 140 | $9.30\times10^{-3}$ | 26.74 | $2.6\times10^{-4}$ | 17.17 | 8.15 |
| $(NH_4)_2SO_4$ | 101 | $1.95\times10^{-2}$ | 42.95 | $2.6\times10^{-4}$ | 28.88 | 3.50 |
| $NH_4HSO_4$ | 57 | $1.14\times10^{-2}$ | 38.43 | $2.6\times10^{-4}$ | 20.17 | 2.83 |

[a]SOA values are the concentrations of SOA on different seeds observed in the experiments. [b]The values of $\gamma$ are consistent with the parameters of the irreversible uptake of MGly used in CMAQ v5.3.[c]$SOA_{MGly}$ is estimated concentration of SOA formed from the irreversible uptake of MGly on different aerosols.

## Reference:


Aiona, P. K., Lee, H. J., Leslie, R., Lin, P., Laskin, A., Laskin, J., and Nizkorodov, S. A.: Photochemistry of products of the aqueous reaction of methylglyoxal with ammonium sulfate, ACS Earth Space Chem., 1, 522-532, 10.1021/acsearthspacechem.7b00075, 2017.

Altieri, K. E., Seitzinger, S. P., Carlton, A. G., Turpin, B. J., Klein, G. C., and Marshall, A. G.: Oligomers formed through in-cloud methylglyoxal reactions: Chemical composition, properties, and mechanisms investigated by ultra-high resolution FT-ICR mass spectrometry, Atmospheric Environment, 42, 1476-1490, 10.1016/j.atmosenv.2007.11.015, 2008.

Bongartz, A., Schweighoefer, S., Roose, C., and Schurath, U.: The mass accommodation coefficient of ammonia on water, Journal of Atmospheric Chemistry, 20, 35-58, 10.1007/bf01099917, 1995.

De Haan, D. O., Pajunoja, A., Hawkins, L. N., Welsh, H. G., Jimenez, N. G., De Loera, A., Zauscher, M., Andretta, A. D., Joyce, B. W., De Haan, A. C., Riva, M., Cui, T. Q., Surratt, J. D., Cazaunau, M., Formenti, P., Gratien, A., Pangui, E., and Doussin, J. F.: Methylamine's Effects on Methylglyoxal-Containing Aerosol: Chemical, Physical, and Optical Changes, Acs Earth and Space Chemistry, 3, 1706-1716, 10.1021/acsearthspacechem.9b00103, 2019.

Fu, T. M., Jacob, D. J., Wittrock, F., Burrows, J. P., Vrekoussis, M., and Henze, D. K.: Global budgets of atmospheric glyoxal and methylglyoxal, and implications for formation of secondary organic aerosols, J. Geophys. Res.: Atmos., 113, D15303, 10.1029/2007jd009505, 2008.

Guo, H., Liu, J., Froyd, K. D., Roberts, J. M., Veres, P. R., Hayes, P. L., Jimenez, J. L., Nenes, A., and Weber, R. J.: Fine particle pH and gas–particle phase partitioning of inorganic species in Pasadena, California, during the 2010 CalNex campaign, Atmos. Chem. Phys., 17, 5703-5719, 10.5194/acp-17-5703-2017, 2017.

Guzmán, M. I., Colussi, A. J., and Hoffmann, M. R.: Photoinduced Oligomerization of Aqueous Pyruvic Acid, The Journal of Physical Chemistry A, 110, 3619-3626, 10.1021/jp056097z, 2006.

Huang, Y., Zhao, R., Charan, S. M., Kenseth, C. M., Zhang, X., and Seinfeld, J. H.: Unified theory of vapor–wall mass transport in Teflon-walled environmental chambers, Environ. Sci. Technol., 52, 2134-2142, 10.1021/acs.est.7b05575, 2018.

Li, Y., Pöschl, U., and Shiraiwa, M.: Molecular corridors and parameterizations of volatility in the chemical evolution of organic aerosols, Atmospheric Chemistry and Physics, 16, 3327-3344,

10.5194/acp-16-3327-2016, 2016.
Li, Y. X., Zhao, J. Y., Wang, Y., Seinfeld, J. H., and Zhang, R. Y.: Multigeneration production of secondary organic aerosol from toluene photooxidation, Environ. Sci. Technol., 55, 8592-8603, 10.1021/acs.est.1c02026, 2021a.
Li, Y. X., Ji, Y. M., Zhao, J. Y., Wang, Y., Shi, Q. J., Peng, J. F., Wang, Y. Y., Wang, C. Y., Zhang, F., Wang, Y. X., Seinfeld, J. H., and Zhang, R. Y.: Unexpected oligomerization of small alpha-dicarbonyls for secondary organic aerosol and brown carbon formation, Environ. Sci. Technol., 55, 4430-4439, 10.1021/acs.est.0c08066, 2021b.
Liu, T. and Abbatt, J. P. D.: Oxidation of sulfur dioxide by nitrogen dioxide accelerated at the interface of deliquesced aerosol particles, Nat. Chem., 13, 1173–1177, 10.1038/s41557-021-00777-0, 2021.
Liu, X., Wang, H., Wang, F., Lv, S., Wu, C., Zhao, Y., Zhang, S., Liu, S., Xu, X., Lei, Y., and Wang, G.: Secondary formation of atmospheric brown carbon in China haze: Implication for an enhancing role of ammonia, Environ. Sci. Technol., 57, 11163-11172, 10.1021/acs.est.3c03948, 2023.
Nah, T., Guo, H., Sullivan, A. P., Chen, Y., Tanner, D. J., Nenes, A., Russell, A., Ng, N. L., Huey, L. G., and Weber, R. J.: Characterization of aerosol composition, aerosol acidity, and organic acid partitioning at an agriculturally intensive rural southeastern US site, Atmospheric Chemistry and Physics, 18, 11471-11491, 10.5194/acp-18-11471-2018, 2018.
Seinfeld, J. H. and Pandis, S. N.: ATMOSPHERIC CHEMISTRY AND PHYSICS: from air pollution to climate change, John Wliey & Sons2006.
Tan, Y., Lim, Y. B., Altieri, K. E., Seitzinger, S. P., and Turpin, B. J.: Mechanisms leading to oligomers and SOA through aqueous photooxidation: insights from OH radical oxidation of acetic acid and methylglyoxal, Atmospheric Chemistry and Physics, 12, 801-813, 10.5194/acp-12-801-2012, 2012.
Tang, M. J., Cox, R. A., and Kalberer, M.: Compilation and evaluation of gas phase diffusion coefficients of reactive trace gases in the atmosphere: volume 1. Inorganic compounds, Atmospheric Chemistry and Physics, 14, 9233-9247, 10.5194/acp-14-9233-2014, 2014.
Tang, M. J., Shiraiwa, M., Pöschl, U., Cox, R. A., and Kalberer, M.: Compilation and evaluation of gas phase diffusion coefficients of reactive trace gases in the atmosphere: Volume 2. Diffusivities of organic compounds, pressure-normalised mean free paths, and average Knudsen numbers for gas uptake calculations, Atmospheric Chemistry and Physics, 15, 5585-5598, 10.5194/acp-15-5585-2015, 2015.
Zhang, X., Cappa, C. D., Jathar, S. H., McVay, R. C., Ensberg, J. J., Kleeman, M. J., and Seinfeld, J. H.: Influence of vapor wall loss in laboratory chambers on yields of secondary organic aerosol, Proc Natl Acad Sci U S A, 111, 5802-5807, 10.1073/pnas.1404727111, 2014.
Zhao, J., Levitt, N. P., Zhang, R. Y., and Chen, J. M.: Heterogeneous reactions of methylglyoxal in acidic media: Implications for secondary organic aerosol formation, Environmental Science & Technology, 40, 7682-7687, 10.1021/es060610k, 2006.